Journal of Applied Polymer Science

Effect of microcellular foaming on the fracture behavior of ABS polymer

Javier Gómez-Monterde,[1,2] Manfred Schulte,[2] Stefan Ilijevic,[2] Jörg Hain,[3] Miguel Sánchez-Soto,[1] Orlando O. Santana,[1] Maria Lluisa Maspoch[1]

[1]Centre Català del Plàstic, Universitat Politècnica de Catalunya-BarcelonaTech (ETSEIB, ETSEIAT), Carrer Colom 114, Terrassa 08222, Spain

[2]Centro Técnico de SEAT SA, Autovía A-2, Km 585, Apartado de Correos 91, Martorell 08760, Spain

[3]Volkswagen AG, D-38436 Wolfsburg, Germany

Correspondence to: J. Gómez-Monterde (E-mail: javier.gomez@upc.edu)

ABSTRACT: In this work, the properties of microcellular ABS were studied. Foamed samples exhibited a solid skin/foamed core structure, with some elongated cells in the flow direction, while spherical cells were mostly observed in the transversal direction. The flexural modulus, flexural strength, and fracture toughness K_{Ic} decreased with the density. However, the *Crack Tip Opening Displacement* (*CTOD*) was found to increase with the foaming ratio. The evolution of the mechanical properties and fracture toughness was well described by prediction models considering the skin/core morphology of these microcellular materials. Foaming increased the anisotropic behavior of the material, due to the cell elongation caused by the fountain flow during injection. © 2015 Wiley Periodicals, Inc. J. Appl. Polym. Sci. **2016**, *133*, 43010.

KEYWORDS: foams; mechanical properties; morphology

Received 30 July 2015; accepted 28 September 2015
DOI: 10.1002/app.43010

INTRODUCTION

Improving fuel efficiency and decreasing greenhouse gasses emissions are the main objectives of the automotive industry. In this regard, researches focus on replacing conventional materials with lighter alternatives, such as polymer/metal hybrid systems, polymer sandwich panels, high performance polymers, reinforced polymer composites, and foamed plastics.

Among the different existing foaming technologies, the microcellular injection molding *MuCell®* process, developed by the *Massachusetts Institute Technology* (*MIT*) in the 1980s, is one of the most promising methods. It consists of dissolving a gas at supercritical pressure and temperature in the melted polymer, forming a single-phase solution. When the mix fills the mold cavity, the pressure drop induces the nucleation of cells, creating a cellular structure in the polymer matrix. Cells sizes are usually lower than 100 μm and cell densities vary from 10^6 to 10^9 cells cm^{-3}. The amount of material is reduced, as well as the cycle time and the requirements of clamping force and processing temperatures. Hence, car parts with reduced weight, cost and carbon footprint can be obtained.[1,2]

Several works have been conducted in order to determine the effect of processing conditions on the morphology and properties in a wide range of materials, such as PP, PE, PC, PS, PET, and reinforced polymers.[3,4] Even biodegradable polymers like PLA[5] and recycled materials such as PET[6] have been investigated in this area. Gibson and Ashby[7] provided an extensive description of the relationship between the cell structure and the governing parameters of the mechanical, thermal, electric, and acoustic behavior. Polymer foams modeling and finite element computations have also been investigated by different authors in the recent years.[8,9]

Nevertheless, fracture behavior of cellular plastics has not been studied in depth yet. Most works have been carried out with rigid plastic foams such as PUR[10] and PVC,[11] whose fracture properties can be determined by the *Linear Elastic Fracture Mechanics* (*LEFM*) theories. When these theories cannot be applied, that is, the material exhibit a ductile behavior and the size of the plastic zone is significant compared to the crack length [*Elastic Plastic Fracture Mechanics* (*EPFM*)], the fracture properties are usually assessed by the *J-integral* and the *Crack Tip Opening Displacement* (*CTOD*) parameters. For highly ductile polymers [*Post Yielding Fracture Mechanics* (*PYFM*)], the *Essential Work of Fracture* (*EWF*) concept is the most common fracture characterization technique.[12,13] However, there is a limited number of researches determining these parameters for cellular materials, such as PP foams.[14]

In this work, Acrylonitrile-Butadiene-Styrene (ABS) polymer was employed. Because of its good mechanical properties, dimensional stability, chemical resistance, good surface appearance, and easy processing and recycling characteristics, it is widely used in engineering applications, such as automotive interior components. As a ductile material, the fracture properties of ABS have been determined mostly by the *EWF* concept. According to Mazidi *et al.*[15] as the rubbery phase content in the ABS material increases, the specific essential work of fracture w_e increases at first, but decreases after passing through a maximum. The plastic work w_p, however, increases with the amount of rubbery phase. They also showed that w_e values can be predicted via the *CTOD* parameter. Many investigations on ABS foaming by batch processes have been made.[16,17] Nevertheless, the fracture behavior of ABS foams has not been extensively investigated yet.

The effect of foaming on the morphology, flexural properties, and fracture behavior was analyzed on plates made of ABS obtained by *MuCell®* microcellular injection molding. It was found that the reduction of mechanical properties and fracture toughness with the foaming ratio can be accurately predicted by models based on the apparent density and the skin/core structure created in the microcellular samples. Foamed specimens presented higher values of the *Crack Tip Opening Displacement* (*CTOD*) parameter than the solid ones, due to the contribution of the cell structure to crack tip blunting.

EXPERIMENTAL

Material

A commercial grade of ABS (*Magnum™ 8434*), supplied by *Styron Netherlands B.V.*, was employed. The material is widely used in automotive interior trims, and has a density of 1.05 g cm^{-3} (ISO 1183/B) and a melt flow index of 13 g/10 min (ISO 1133).

Injection Molding

The ABS was dried at 80°C for a minimum of 4 h in a *DSN560HE* dehumidifier (*PIOVAN*) with a dew point of −40°C, before the injection molding experiments.

Square plates of 100 × 100 × 5 mm^3 were produced in a *Victory 110* injection molding machine (*Engel GmbH*), with a clamping force of 1100 kN and equipped with the *MuCell®* supercritical fluid (*SCF*) supply system. A constant melt temperature profile from hopper to nozzle of 160–220–230–245–250°C was employed, and the mold temperature was kept at 60°C. Solid and foamed plates with 10 and 17% of weight reduction were obtained by varying the shot volume from 70.0 to 50.1 and 46.2 cm^3, respectively. Gas N_2 was used as physical blowing agent, with a gas content of 0.53 and 0.58% for the two ratios of weight reduction. The selected injection speed for the solid plates was 50 cm^3 s^{-1}, whereas it was 80 cm^3 s^{-1} for the foamed samples.

Characterization

Morphology and Apparent Density. The morphology was analyzed in 10 mm width cross sections of the plates taken at different distances from the injection gate (15, 50, and 85 mm) both in a parallel (MD) and transversal direction (TD) to the injection flow. Prior to observation, the specimens were cryogenically fractured. The resulting fracture surfaces were examined by Scanning Electron Microscopy (SEM) with a *JEOL JSM-560* microscope. Quantitative parameters such as cell size, cell density, and skin thickness were determined with the help of *Igor Pro®* (*Wavemetrics Inc.*) and *Matlab®* (*The MathWorks Inc.*) software, after adjusting the micrographs for appropriate level of contrast. Cell density (N) is referred as the number of cells per volume (cells cm^{-3}), and it is calculated as follows:

$$N = \left(\frac{n}{A}\right)^{\frac{3}{2}} \left(\frac{\rho_s}{\rho_f}\right) \quad (1)$$

Where n is the number of cells in the micrograph, A is the analyzed area (cm^2), and ρ_s and ρ_f are the density of solid and foamed material.

The apparent density of the plates and different sections of the morphological analysis was calculated by weighing and measuring the dimensions with a digital caliper.

Flexural Properties. Flexural tests were carried out in 100 × 10 × 5 mm^3 specimens machined out of the square plates. To relate the flexural properties with the cell structure determined by morphology analysis, the same distances from the injection gate and orientations were employed. Experiments were done following the ISO 178 standard, in a *Galdabini Sun 2500* testing machine with a span length of 80 mm, at a crosshead speed of 10 mm min^{-1} and at room temperature. At least five samples of solid and foamed plates were tested for each material, position and direction.

Fracture Behavior. The fracture behavior of the solid and foamed plates was characterized at low loading speed by the *Crack Tip Opening Displacement* (*CTOD*), as well as at high testing rate by the fracture toughness (K_{Ic}).

SENT (*Single Edge Notched Tension*) specimens were employed to determine the *CTOD* parameter, whose size and dimensions are plotted in Figure 1. The notch length/width ratio (*a/W*) was kept as 0.6, in order to avoid triaxial stress states at the crack tip.[18] The low speed tests were performed using a *Zwick/Roell* universal testing machine, *Amsler HC25/2008* model, at a crosshead rate of 16 mm min^{-1}. The tests were recorded by two digital cameras at a frame rate of 10 pictures per second (*Xenoplan 1.4/23-0.902*, *Schneider Kreuznach*) coupled to a *GOM/ARAMIS* digital image correlation system. The *CTOD* parameter was calculated by measuring the displacement of the notch faces at the crack propagation onset.

The fracture toughness of the solid and foamed ABS was assessed through *SENB* (*Single Edge Notched Bending*) specimens, as shown in Figure 1. According to the testing protocol,[19] the *a/W* ratio was in the range of $0.45 \leq a/W \leq 0.55$. The impact tests were carried out using an instrumented *CEAST Resil* impactor, equipped with a 15J hammer. The pendulum had a length of 0.374 m and a reduced mass of 3.654 kg, and it was impacted at an angle of 30°. The fracture toughness was calculated as follows:

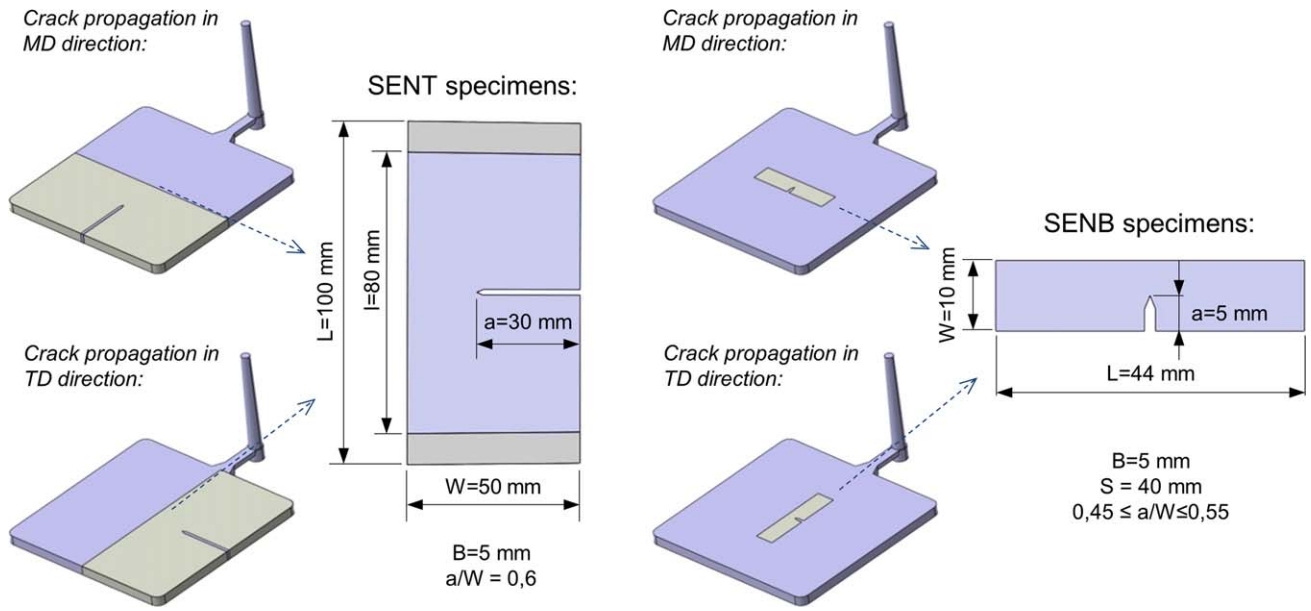

Figure 1. Scheme of *SENT* and *SENB* specimens machined out from the injected plates. [Color figure can be viewed in the online issue, which is available at wileyonlinelibrary.com.]

$$K_{Ic} = f\frac{P_q}{B\sqrt{W}} \quad (2)$$

Where P_q is the calculation force (N), B and W are the part thickness and width (mm) respectively, and f is a geometric function depending on the a/W ratio and determined according to the aforementioned protocol.[19]

All fracture tests were performed at room temperature and the notch was sharpened by sliding a razor blade. The specimens were extracted from the injected plates, ensuring the correspondence between the crack propagation sections and the morphology analyzed in the middle of the plates. At least five specimens were tested for each material, orientation and loading speed.

RESULTS AND DISCUSSION

Morphology and Apparent Density

Figures 2 and 3 show SEM micrographs taken from different sections and directions of both foamed plates groups. According to these pictures, the material structure consisted of two solid skins and a foamed core, typical of cellular polymers obtained by injection molding. Near the injection point (MD-A), cells were spherical and uniformly distributed through the foamed core.

However, cells became distorted as the distance away from the injection gate became larger (MD-C). Dong *et al.*[20] explained this phenomenon as the result of the two mechanisms involved in the cell forming process: *foaming during filling* and *foaming after filling*. At the beginning of the filling stage, the fast pressure drop leads to the nucleation of a large number of cells. Cells near the melt front are distorted by the fountain-flow behavior of the melt. This cell forming process is called *foaming during filling*. As the mold cavity gets filled, the pressure increases up to a critical point at which the polymer melt is just not supersaturated of gas, and foaming does not take place. Finally, once the filling stage is finished, the melt pressure drops again during cooling and spherical cells are formed at the beginning of the part. This second mechanism is known as *foaming after filling*. In TD direction, however, cells presented a mainly spherical shape along the whole foamed core.

The morphological parameters (solid skin, cell density and cell size range) determined from details of Figures 2 and 3 are displayed in Table I. In general, there are no significant variances in the morphology parameters between the two levels of weight reduction and between the different analyzed sections, either in parallel (MD) or transversal (TD) direction to the melt front. However, an increase in the solid skin along the flow direction can be noticed. As explained by Dong *et al.*,[21] the solid surface layers formation is also submitted to the different mechanisms during filling and after filling, and it is expected a thinner solid skin near the gate and an increase in thickness with the distance to the injection gate, with a maximum value in the center of the part.

The cell density is kept in an order of magnitude of 10^7 cells cm^{-3} in all cases. Tsuchiya *et al.*[22] stated that the butadiene rubber in ABS acts as foaming nucleus, which justifies the high cell density and the homogeneous cell distribution observed. The cell size is contained in a range of 6–47 μm, which is in the same order as the average diameter (50 μm) obtained in ABS foams produced by combining chemical and physical foaming processes at the same time.[23] As a general trend, foamed plates with 17% of weight reduction present slightly higher cell densities and narrower cell size ranges. The ability of cell nucleation increases with the content of supercritical fluid agent, as has been found in PEI[24] and PS foams.[25] Nevertheless, the morphology examination at a macroscopic scale revealed a greater presence of bigger cells (150–250 μm) in this group of foamed plates, due to a higher gas content and cell coalescence. As a consequence, the overall apparent density decreases from 1.03 g cm^{-3} of the solid samples to 0.93 g cm^{-3} (10% of weight reduction) and 0.86 g cm^{-3} (17% of weight reduction). Positions far from the injection gate

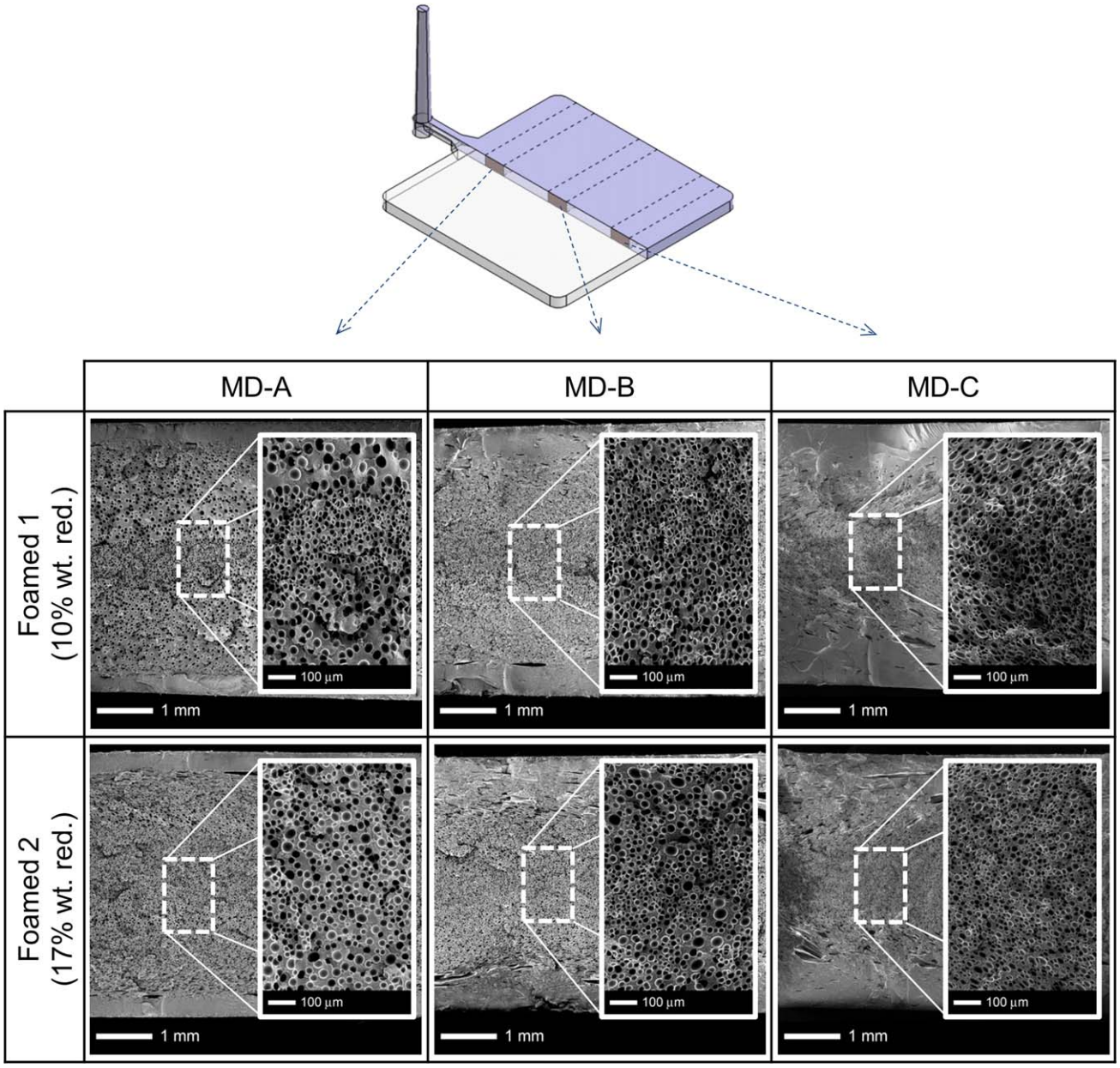

Figure 2. SEM micrographs of foamed ABS plates taken in MD direction. [Color figure can be viewed in the online issue, which is available at wileyonlinelibrary.com.]

are slightly denser than those close to the beginning areas (Table II), which could be explained because of the higher skin/core ratio. A similar trend has been observed in Ethylene-Propylene Block Copolymer (EPBC) foams.[26]

Flexural Properties

The results obtained from the flexural tests of solid and foamed specimens are illustrated in Figure 4(a–d). All the specimens reached a maximum stress but did not break before the conventional deflection given by the ISO 178 standard.

As a consequence of the density reduction, the flexural modulus was diminished by around 12 and 23% (10 and 17% of weight reduction) in samples extracted in MD direction, whereas it was decreased by 13 and 20% in the opposite orientation. Flexural strength, however, experimented a greater reduction ratio, with reductions of 22 and 32% in case of specimens tested in MD direction, and 19 and 25% in TD samples. In all cases, the gap between properties of solid and foamed specimens was strongly reduced when the specific values were calculated [solid line in Figure 4(a–d)]. The specific flexural modulus of the 10% of weight reduction foamed specimens even exceeded the specific modulus of the unfoamed plates.

A slight reduction in the flexural modulus and strength of solid samples can be observed in MD direction, which might be due to a slight decrease in the packing pressure at the end of the cavity. Nevertheless, foamed samples presented the opposite

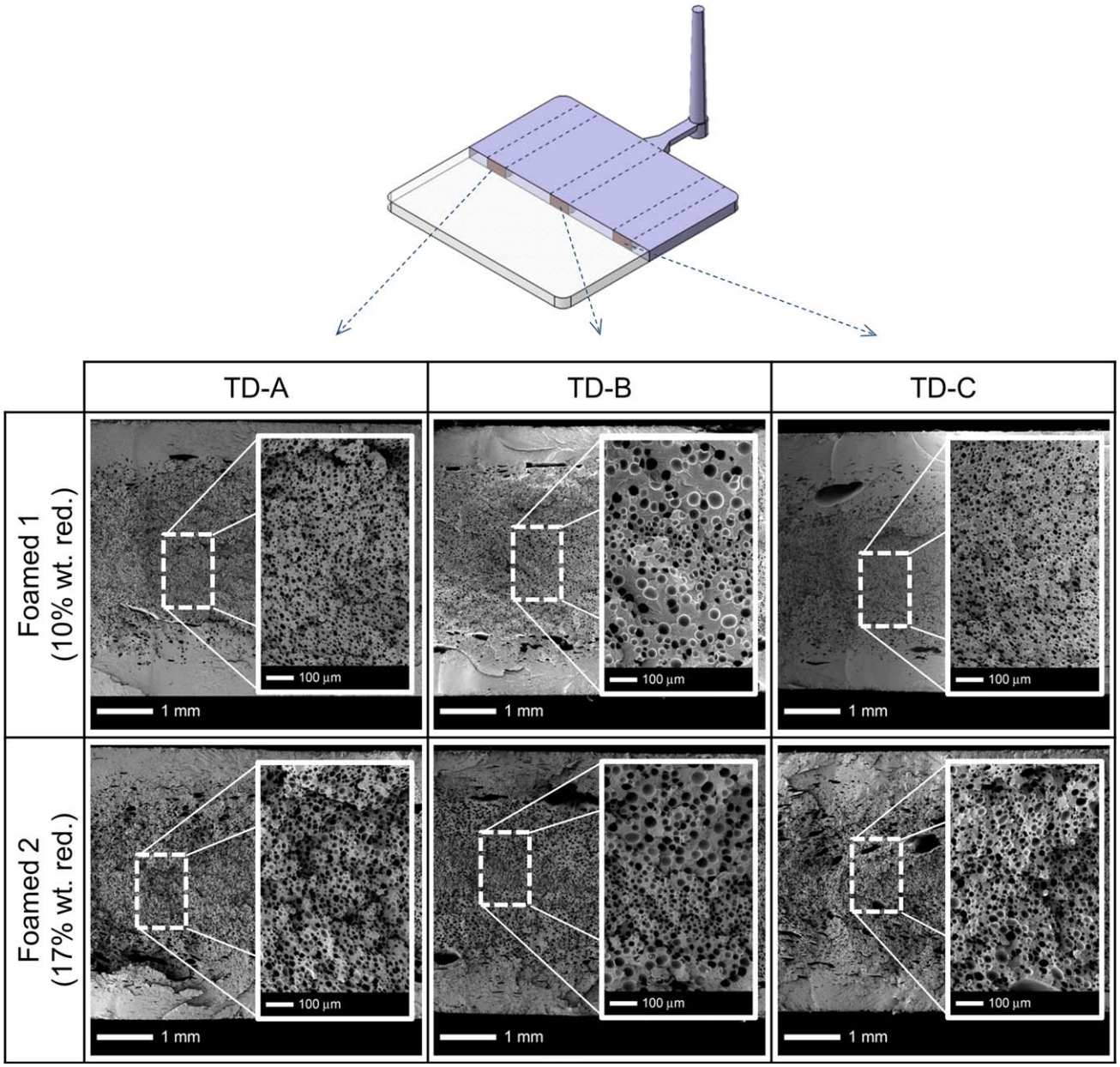

Figure 3. SEM micrographs of foamed ABS plates taken in TD direction. [Color figure can be viewed in the online issue, which is available at wileyonlinelibrary.com.]

trend, with higher flexural modulus and strength at the end areas, as also reported by Rezavand *et al.*[27] This tendency could be due to the thicker skin layers. When samples are taken in TD direction, no great differences are detected in the three tested sections, because of the more homogeneous morphology generated in the center of the plate.

The two levels of foamed samples present differences in flexural strength of 7 and 12%, respectively, when MD and TD directions are compared. This variation cannot be only attributed to the material orientation, but also to the influence of the elongation of the cells observed in the morphology analysis.

When load is applied in a bending test, the upper side of the specimen is compressed, while the lower surface is in tension. Therefore, the solid skins play an important role on the flexural performance of foams, as well as the density. Zhang *et al.*[28] developed the Square-Power law model, simplifying the structural foam as a three-layer sandwich. Hence, the normalized modulus is given as:

$$\frac{E_{ff}}{E_{fs}} = \left[1 - \left(1 - \left(\frac{\rho_f}{\rho_s}\right)^2\right)\left(1 - \frac{t_1 + t_2}{h}\right)^3\right] \quad (3)$$

Where E_{ff}, E_{fs}, ρ_f, and ρ_s are the flexural modulus and apparent density of foamed and solid material, respectively. The variables t_1 and t_2 are the skin thickness of both surface layers, and h is the overall part thickness. Taking average values of skin thickness, apparent density and flexural properties of the solid material, the predicted flexural modulus was 1913 MPa (10% of weight

Table I. Morphological Parameters of Foamed Samples

Material	Section	Skin thickness (mm)	Cell density (cells cm^{-3})	Cell size range (μm)	Average cell size (μm)
Foamed 1 (10% wt red.)	MD-A	0.36	1.1×10^7	17-47	26
	MD-B	0.52	6.7×10^7	8-22	15
	MD-C	0.66	7.3×10^7	9-25	13
	TD-A	0.65	6.2×10^7	7-16	12
	TD-B	0.63	1.8×10^7	12-33	17
	TD-C	0.58	6.7×10^7	7-18	12
Foamed 2 (17% wt red.)	MD-A	0.38	1.9×10^7	15-34	20
	MD-B	0.46	4.2×10^7	9-30	18
	MD-C	0.52	9.9×10^7	6-24	15
	TD-A	0.49	7.0×10^7	5-20	12
	TD-B	0.50	2.0×10^7	5-29	17
	TD-C	0.49	3.8×10^7	6-25	16

reduction) and 1780 MPa (17% of weight reduction), with a maximum deviation from the experimental results of 8%.

On the other hand, Xu and Kishbaugh[29] proposed a model to estimate the flexural strength of microcellular plastics considering the skin/core complex structure:

$$\frac{\sigma_{ff}}{\sigma_{fs}} = \frac{2t^3}{h^3} + \frac{6t(h\text{-}t)^3}{h^3} + (1\text{-}R)^2 \left(\frac{h\text{-}2t}{h}\right)^3 \quad (4)$$

In eq. (4), t is the solid skin thickness, h is the overall part thickness, and R is the real weight reduction ratio in the foamed core, calculated as a function of t and h thicknesses and the weight reduction ratio of the whole part (R_w):

$$R = \frac{h(1\text{-}R_w)}{h\text{-}2t} \quad (5)$$

In this case, the estimated flexural strengths obtained were 61.7 and 57.2 MPa for 10 and 17% levels of weight reduction ($R_w = 0.10$ and 0.17). The maximum deviation with regard to the experimental results in MD direction is around 21%, and 8% in TD specimens. This difference in the accuracy of the model is due to the anisotropy induced by the addition of gas, which is not considered in the model. Cell density and size also influence the mechanical properties of the foam. According to Li *et al.*,[30] low cell sizes have a positive effect on the flexural modulus and strength. In the present study, the achieved fine cell structures pointed out toward maximum values of flexural properties.

Fracture Behavior

Crack Tip Opening Displacement *CTOD*. Figure 5(a) shows the force versus displacement plots obtained with *SENT* solid and foamed specimens tested in TD direction. In all materials, crack propagation initiates before reaching the maximum force, and before undergoing full ligament yielding. Additionally, crack propagation was not stable along the whole ligament. This behavior suggests that the stress state ahead of the crack tip was possibly not pure plane stress due to the relative large sample thickness (i.e., 5 mm); probably leading to unstable crack propagation. Therefore, the application of the *Essential Work of Fracture* (*EWF*) method is not fully accurate for characterizing the fracture behavior of these solid and foamed ABS samples. On this basis, the *Crack Tip Opening Displacement* (*CTOD*) concept was used in the current work in order to evaluate the fracture behavior of these materials.

Table III summarizes the results determined from the low loading speed tests. The *CTOD* value of both foamed samples was higher than the solid ones and increased with the gas content (i.e., 12 and 30% in case of 10 and 17% of weight reduction levels, respectively). As expected, cells act as crack arrestors by blunting the crack tip. Thus, the crack propagation onset is delayed and a higher *CTOD* value is obtained. The strain field ahead of the crack tip was determined at the crack propagation onset using digital image correlation technique. As shown in Figure 5(a), the size of the plastic zone cannot be neglected as compared to the ligament length, due to the ductile behavior of

Table II. Apparent Densities Measured in Different Sections of the Plates

	Density (g cm^{-3})					
Material	MD-A	MD-B	MD-C	TD-A	TD-B	TD-C
Solid	0.98 ± 0.02	0.99 ± 0.03	0.96 ± 0.03	1.01 ± 0.03	1.01 ± 0.02	1.01 ± 0.02
Foamed 1 (10% wt red.)	0.80 ± 0.04	0.81 ± 0.03	0.91 ± 0.03	0.83 ± 0.04	0.84 ± 0.03	0.85 ± 0.03
Foamed 2 (17% wt red.)	0.75 ± 0.01	0.78 ± 0.01	0.76 ± 0.05	0.78 ± 0.02	0.78 ± 0.01	0.79 ± 0.03

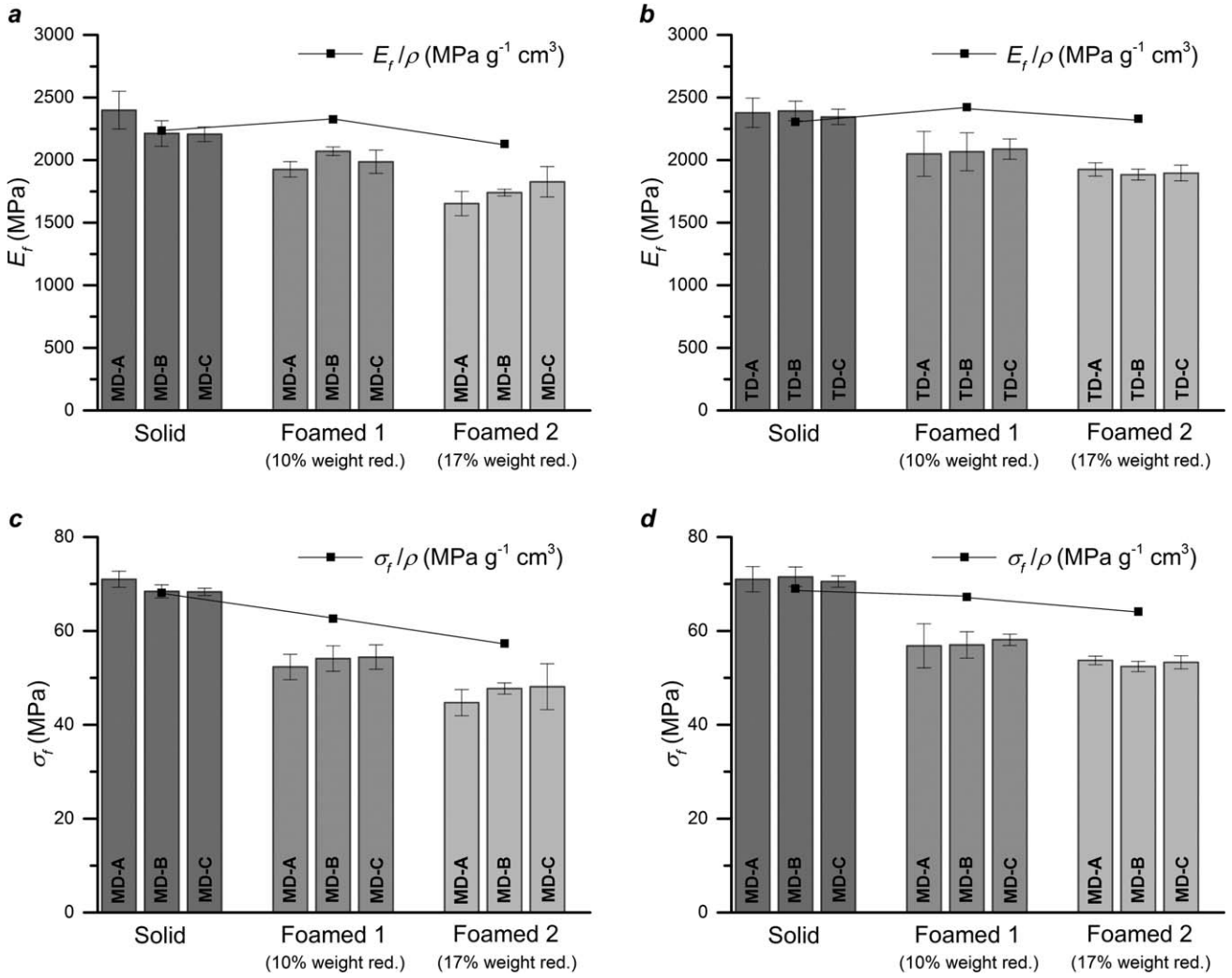

Figure 4. (a) Flexural modulus of samples tested in MD direction; (b) Flexural modulus of samples tested in TD direction; (c) Flexural strength of samples tested in MD direction; (d) Flexural strength of samples tested in TD direction. Solid line in graphs represents specific flexural properties.

the ABS material. In the foamed samples, the higher *CTOD* values gave rise to an increase in the maximum strain levels.

In case of the solid samples, no significant differences between the *CTOD* values obtained in MD and TD directions were detected. However, in the foamed specimens the *CTOD* determined in TD direction was slightly higher than in MD, due to the increased anisotropy caused by the gas introduction.

Regarding the crack propagation process, in solid specimens the crack tended to propagate in a stable manner along a straight line up to a ligament length of around 10 mm, when catastrophic failure took place [Figure 5(c,d)]. In the foamed samples, however, the crack propagation can be considered quasi-stable, due to the subsequent processes of deformation, rupture, and cell coalescence. In the foam structure, the crack tends to surround the cells prior to propagation. Therefore the crack path is certainly not a straight line. In addition, once the crack starts to propagate, secondary cracks arise ahead of the main crack front which grow and coalesce, triggering a faster crack propagation process [Figure 5(f–i)]. The same phenomenon has been reported in PVC and PES foams although under fatigue cycle load conditions.[31] All of the above justifies the quasi-stable character of the crack propagation in different planes observed in the foamed specimens. The maximum extension of this quasi-stable crack propagation before unstable failure is similar to that of the solid material (10 mm).

Fracture Toughness K_{Ic}. The fracture toughness K_{Ic} results of the high speed tests are outlined in Table III. The values obtained in the solid material are consistent with those provided by the *European Structural Integrity Society* (*ESIS*) for ABS[19] and slightly lower than the obtained at slow loading speed on 10-mm thick samples.[32]

According to Bureau and Kumar,[33] cells act as stress concentrators at the crack tip due to stress triaxiality, thus a reduction in the fracture toughness is expected in foamed materials. Table III points out a decrease in the fracture toughness with the weight reduction ratio, as a consequence of lower density, resistance, and energy absorption capability. The same trend has been reported for PVC and PES foams.[34]

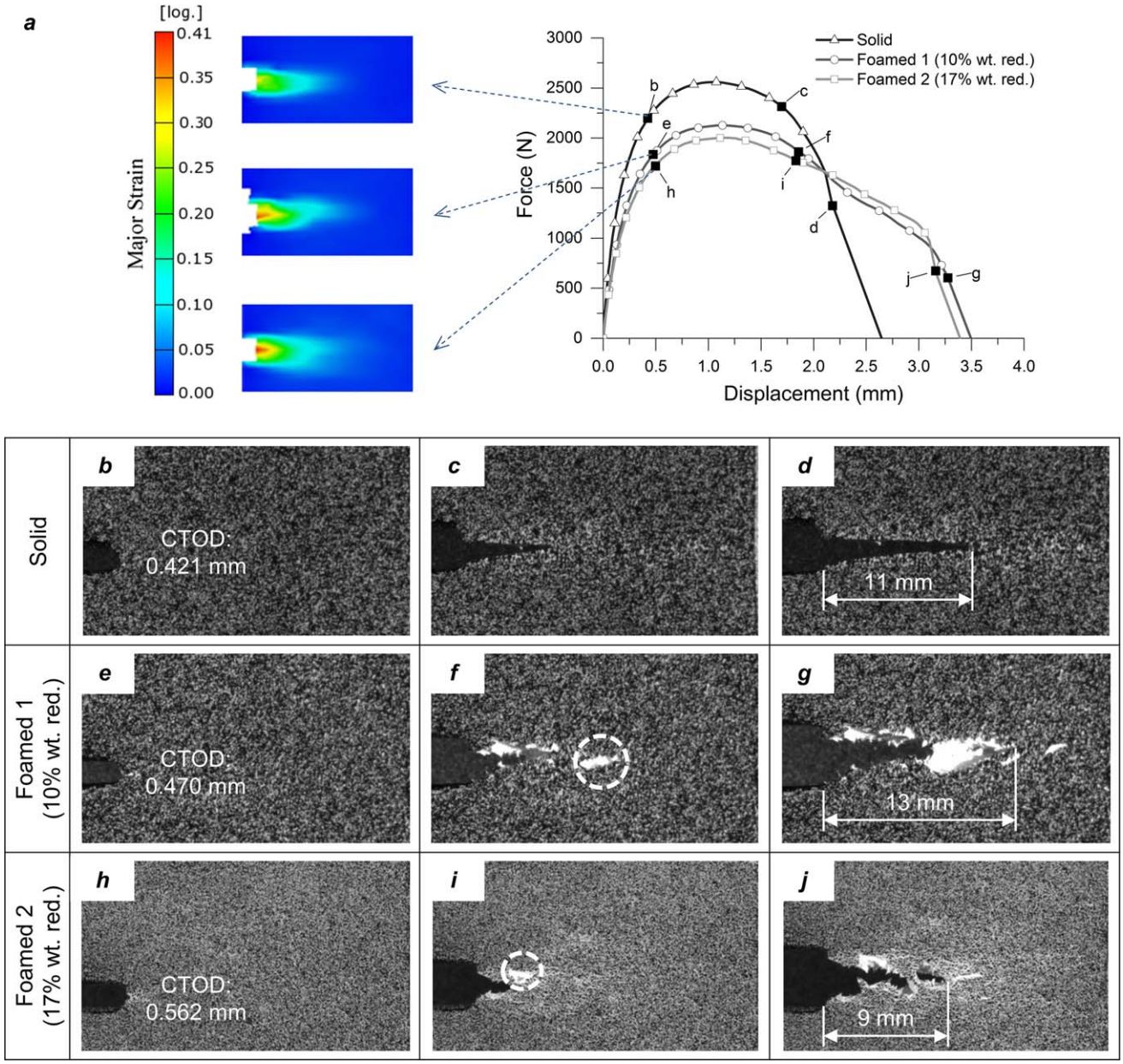

Figure 5. (a) Strain field ahead of the crack tip at the crack propagation onset and Force-displacement curves for solid and foamed samples tested in TD direction at 16 mm min^{-1}; (b, e, h) Micrographs taken at the crack propagation onset with the corresponding *CTOD* value; (c) Stable crack propagation of solid samples; (f, i) Quasi-stable crack propagation of foamed samples with secondary cracks ahead of the main crack front, indicated into the white dashed circles; The stable crack propagation length is indicated in figures (d, g, j) for each material investigated before the catastrophic crack propagation. [Color figure can be viewed in the online issue, which is available at wileyonlinelibrary.com.]

As observed in the *CTOD* parameter, foaming promotes a higher anisotropic material behavior, with higher fracture toughness when the crack propagates in TD direction. To get a better insight into the different behavior of the foams according to the crack propagation orientation, the fracture surfaces were examined using Scanning Electron Microscopy (SEM). It is well known that ABS failure is governed by rubber particles cavitation and shear-yielding. However, in the presence of a sharpened notch, the notch itself dominates the crack propagation and the fracture process. The fracture surfaces of the solid samples and 10% weight reduction foams are illustrated in Figure 6. It can be seen that there was no significant differences between the fracture surfaces of solid specimens. In case of the cellular material, the surfaces shown in Figure 6 presented similar solid thicknesses and a smooth surface, which evidenced a brittle failure. Moreover, the notches spread over the whole part thickness. However, in the surface obtained when the crack propagated in MD direction, cells were elongated and distorted as discussed in the morphology analysis, while fracture surfaces corresponding to TD direction exhibited more spherical cells. This difference in the cell shape could explain the differences in the fracture behavior according to the crack propagation direction.

Table III. *CTOD* and Experimental and Predicted K_{Ic}

Material	Crack propagation direction	*CTOD* (mm)	Experimental K_{Ic} (MPa m$^{-1/2}$)	Prediction model 1 K_{Ic} (MPa m$^{-1/2}$)	Prediction model 1 Error (%)	Prediction model 2 K_{Ic} (MPa m$^{-1/2}$)	Prediction model 2 Error (%)
Solid	MD	0.434 ± 0.014	3.34 ± 0.30	-	-	-	-
	TD	0.444 ± 0.015	3.36 ± 0.16		-		-
Foamed 1 (10% wt red.)	MD	0.481 ± 0.032	1.94 ± 0.18	2.24	15.3	2.22	15.6
	TD	0.497 ± 0.028	2.23 ± 0.19		0.5		0.1
Foamed 2 (17% wt red.)	MD	0.504 ± 0.021	1.68 ± 0.14	1.99	19.0	1.98	18.3
	TD	0.564 ± 0.030	1.95 ± 0.16		2.4		1.8

Finally, two estimation models for predicting the K_{Ic} parameter were applied. The Model 1 is used by Kabir *et al.*,[35] and relates the relative fracture toughness to the relative foam density through a power law as described in eq. (6):

$$\frac{K_{Ic,f}}{K_{Ic,s}} = C\left(\frac{\rho_f}{\rho_s}\right)^n \tag{6}$$

Taking the values of $C = 1$ and $n = 2$, the resulting model is analog to the equations to predict the tensile and flexural properties of the cellular materials. The estimated K_{Ic} values are shown in Table III. As can be seen, the model fits well to the experimental K_{Ic} obtained in TD direction of crack propagation, but the error is around 15–20% compared to that of MD direction.

The Model 2 was suggested by Maiti *et al.*,[36] and it considers additional parameters such as the strength of the cell walls in bending σ_{fs} and the average cell size d:

$$\frac{K_{Ic,f}}{K_{Ic,s}} = C\sigma_{fs}\sqrt{\pi d}\left(\frac{\rho_f}{\rho_s}\right)^m \tag{7}$$

In this case, the best fitting value for the C constant was 2, the average flexural strength of the solid ABS σ_{fs} was 70 MPa, and the average cell size d was 16 μm. The exponent m took a value of 2, as proposed by the authors for closed cell structures. Table III shows the predicted fracture toughness obtained applying this second model. It is quite accurate for the experimental values in TD direction, but the error when the MD results are considered is similar to that of the Model 1. In conclusion,

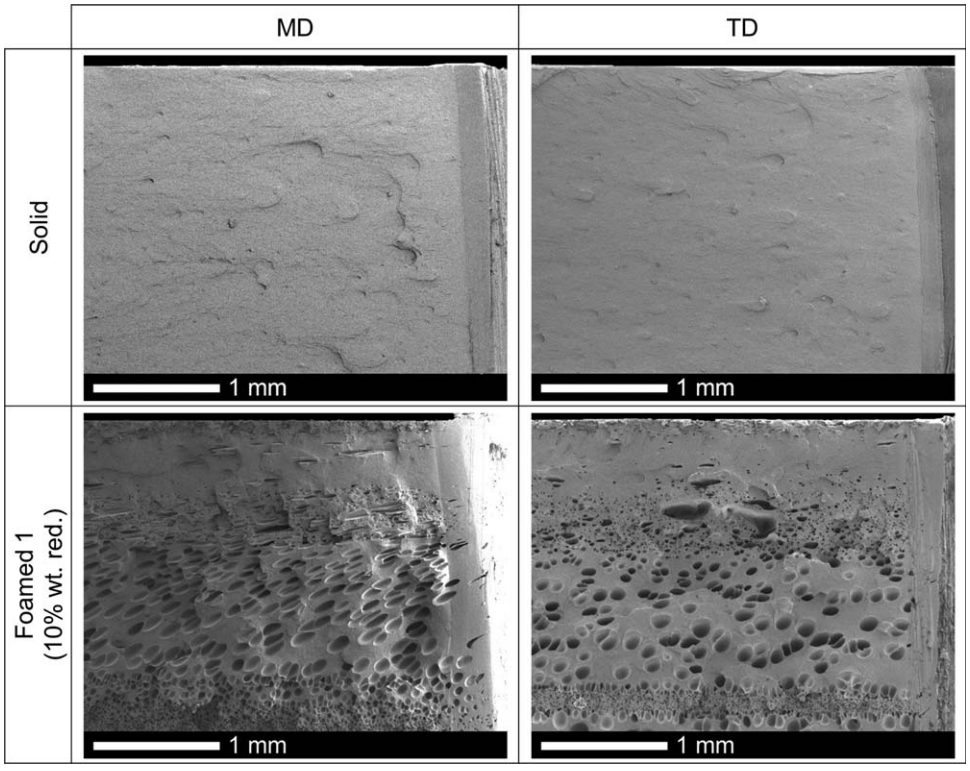

Figure 6. Fracture surfaces of solid and foamed samples in MD and TD direction.

these two models are well adjusted with foams having perfect spherical cell shapes, but they deviate from the experimental results when cells are elongated and distorted.

CONCLUSIONS

In this work, ABS was used to inject solid and foamed square plates with two levels of weight reduction (10 and 17%). Foamed specimens presented a solid skin/foamed core structure. The morphology examined in parallel direction to the melt flow exhibited some distorted and elongated cells, while most cells in the cross section had a spherical shape. Regarding the mechanical properties, both flexural modulus and strength decreased with the density of the foamed samples. Prediction models employed to estimate the evolution of the relative flexural modulus with the relative density fitted accurately to the experimental data.

The fracture behavior was characterized by the *Crack Tip Opening Displacement* parameter at low loading speed tests, as well as by fracture toughness K_{Ic} at high loading rates. The *CTOD* parameter increased with the foaming ratio because cells acted as crack arrestors by blunting the crack tip. However, the fracture toughness K_{Ic} decreased with the density of the samples. The fracture toughness K_{Ic} was well described by a simple power law equation as well as by a more complex model considering flexural properties and cell size.

Foaming increased the anisotropic behavior of the material, obtaining higher flexural properties, *CTOD*, and fracture toughness K_{Ic} in the cross direction to the melt flow. The cell elongation due to the fountain flow in the injection direction seemed to be the most likely reason for this different performance.

ACKNOWLEDGMENTS

The authors are grateful to Ministerio de Economía y Competitividad from Spain for the MAT 2013-40730P project. J. Gómez-Monterde thanks the Government of Catalonia and Rücker Lypsa S.L.U. for their collaboration in the Industrial Doctorate Plan.

REFERENCES

1. Elduque, D.; Claveria, I.; Fernandez, A.; Javierre, C.; Pina, C.; Santolaria, J. *Adv. Mech. Eng.* **2014**, *6*, 793269.
2. Kim, H. C.; Wallington, T. *J Environ. Sci. Technol.* **2013**, *47*, 6089.
3. Rizvi, S. J. A.; Bhatnagar, N. *Int. Polym. Proc.* **2009**, *24*, 399.
4. Bledzki, A. K.; Faruk, O.; Kirschling, H.; Kuhn, J.; Jaszkiewicz, A. *Polimery* **2007**, *52*, 3.
5. Ameli, A.; Nofar, M.; Jahani, D.; Rizvi, G.; Park, C. B. *Chem. Eng. J.* **2015**, *262*, 78.
6. Srithep, Y.; Turng, L. S. *J. Polym. Eng.* **2014**, *34*, 5.
7. Gibson, L. J.; Ashby, M. F. Cellular Solids: Structure and Properties; Cambridge University Press: Cambridge, **1999**; p 532.
8. Natesaiyer, K.; Chan, C.; Sinha-Ray, S.; Song, D.; Lin, C. L.; Miller, J. D.; Garboczi, E. J.; Forster, A. M. *J. Mater. Sci* **2015**, *50*, 4012.
9. Srivastava, V.; Srivastava, R. *J. Mater. Sci.* **2014**, *49*, 2681.
10. Marsavina, L.; Sadowski, T. *Polym. Test.* **2008**, *27*, 941.
11. Poapongsakorn, P.; Carlsson, L. A. *Compos. Struct.* **2013**, *102*, 1.
12. Martinez, A. B.; Gamez-Perez, J.; Sanchez-Soto, M.; Velasco, J. I.; Santana, O. O.; Maspoch, M. L. *Eng. Fail. Anal.* **2009**, *16*, 2604.
13. Barany, T.; Czigany, T.; Karger-Kocsis, J. *Prog. Polym. Sci.* **2010**, *35*, 1257.
14. Arencon, D.; Antunes, M.; Martinez, A. B.; Velasco, J. I. *Polym. Test.* **2012**, *31*, 217.
15. Mazidi, M. M.; Aghjeh, M. K. R. A. F. *J. Mater. Sci.* **2012**, *47*, 6375.
16. Nadella, K.; Kumar, V. In Experimental Analysis of Nano and Engineering Materials and Structures; Springer: Dordrecht (Netherlands), **2007**; p 765.
17. Nadella, K.; Kumar, V.; Li, W. *Cell. Polym.* **2005**, *24*, 71.
18. Anderson, T. L. Fracture Mechanics: Fundamentals and Applications; CRC press: Boca Raton (USA), **2005**; p 640.
19. Moore, D. R.; Williams, J. G.; Pavan, A. Fracture Mechanics Testing Methods for Polymers, Adhesives and Composites; Elsevier, ESIS Publication: Oxford (UK), **2001**; Vol. *28*, p 388.
20. Dong, G. W.; Zhao, G. Q.; Guan, Y. J.; Wang, G. L.; Wang, X. X. *J. Appl. Polym. Sci.* **2014**, *131*, 40365.
21. Dong, G.; Zhao, G.; Guan, Y.; Li, S.; Wang, X. *J. Cell. Plast.* **2015**. doi: 10.1177/0021955X15577149.
22. Tsuchiya, A.; Tateyama, H.; Kikuchi, T.; Takahashi, T.; Koyama, K. *Polym. J.* **2007**, *39*, 514.
23. Seo, J. H.; Han, J.; Lee, K. S.; Cha, S. W. *Polym. Plast. Technol.* **2012**, *51*, 455.
24. Liu, T.; Lei, Y. J.; Chen, Z. L.; Wang, X. Z.; Luo, S. K. *J. Appl. Polym. Sci.* **2015**, *132*, 41443.
25. Chen, S. C.; Hsu, P. S.; Hwang, S. S. *J. Appl. Polym. Sci.* **2013**, *127*, 4769.
26. Gomez-Gomez, J. F.; Arencon, D.; Sanchez-Soto, M. A.; Martinez, A. B. *Adv. Polym. Technol.* **2013**, *32*, E692.
27. Rezavand, S. A. M.; Behravesh, A. H.; Mahmoodi, M.; Shahi, P. 25th Annual Meeting of the Polymer Processing Society, Goa (India), **2009**.
28. Zhang, Y.; Rodrigue, D.; Ait-Kadi, A. *J. Appl. Polym. Sci.* **2003**, *90*, 2139.
29. Xu, J.; Kishbaugh, L. *J. Cell. Plast.* **2003**, *39*, 29.
30. Li, J. L.; Chen, Z. L.; Wang, X. Z.; Liu, T.; Zhou, Y. F.; Luo, S. K. *J. Appl. Polym. Sci.* **2013**, *130*, 4171.
31. Saenz, E. E.; Carlsson, L. A.; Karlsson, A. M. *Eng. Fract. Mech.* **2013**, *101*, 23.
32. Oskui, A. E.; Choupani, N.; Haddadi, E. *Polym. Eng. Sci.* **2014**, *54*, 2086.
33. Bureau, M. N.; Kumar, V. *J. Cell. Plast.* **2006**, *42*, 229.
34. Saenz, E. E.; Carlsson, L. A.; Karlsson, A. *J. Mater. Sci.* **2011**, *46*, 3207.
35. Kabir, M. E.; Saha, M. C.; Jeelani, S. *Mater. Sci. Eng. A Struct.* **2006**, *429*, 225.
36. Maiti, S. K.; Ashby, M. F.; Gibson, L. J. *Scr. Metall. Mater.* **1984**, *18*, 213.